Article:
Miller, D., Viswanathan, V., Tiwari, D. et al. (2025) Monitoring of Argon plasma in a coating manufacturing process by utilising IR imaging techniques. Journal of Manufacturing Processes, 138. pp. 79-89. ISSN: 1526-6125

https://doi.org/10.1016/j.jmapro.2025.01.093

Monitoring of Argon plasma in a coating manufacturing process by utilising IR imaging techniques

David Miller[a,e], V. Viswanathan[b], Divya Tiwari[a], Windo Hutabarat[a], Saurav Goel[b,d,f], Beth Muthoni Irungu[b], Allan Matthews[c], Ashutosh Tiwari[a]

[a]*Automatic Control and Systems Engineering, The University of Sheffield, Sheffield, S1 3JD, UK*
[b]*School of Engineering, London South Bank University, London, SE1 0AA, UK*
[c]*Department of Materials, The University of Manchester, Manchester, M13 9PL, UK*
[d]*University of Petroleum and Energy Studies, Dehradun, 248007, India*
[e]*Sheffield Corresponding Author: d.b.miller@sheffield.ac.uk +447742706468*
[f]*LSBU Corresponding Author: goels@lsbu.ac.uk*

Abstract

Atmospheric plasma spray is a complex multivariable manufacturing process used in a wide range of industries. Deviations in the process parameters have been shown to affect the coating quality. Currently, the quality analysis is performed at the end of the process rather than checking for defects during the process. However, monitoring for these deviations during a coating process is difficult due to environmental hazards such as UV radiation, dusty environment, and excessive noise generation. A commercially available thermal imaging camera was integrated into this space to directly monitor the atmospheric plasma heat distribution and its influence on the in-flight particle trajectories during spraying. A novel metric called asymmetric angle is proposed to monitor the asymmetry of the plasma heat distribution. This is an important metric as a symmetric heat distribution is required to heat all the particles adequately to form a good quality coating. Further metrics of

Gaussian Aspect Ratio (GAR) and contour area were found to have a relationship with the plasma gas flow rate and are discussed. The spray angle of the material is also tracked by fitting a 1D line to the regional Shannon entropy of the thermal image. The limitations of these metrics are discussed with possible avenues of further investigation.
Keywords: coating processes, process monitoring, thermal imaging

---

1. Introduction

In-process monitoring of products and processes during manufacturing has gained prominence for improving quality, sustainability and repeatability [1, 2]. Surface Engineering has evolved from being an aesthetic, surface hardening method to a functional requirement depending upon the applications where it is used [3, 4].

A growing number of manufacturing methods and techniques are leading to a new avalanche of opportunities in deposition methods however when it concerns the fabrication of engineering components to be used in harsh chemical and thermal environments, thermal spray continues to have its dominance in the sector [5, 6].

Plasma spray is a process in which a plasma arc is generated between a negatively charged electrode and a positively charged nozzle. An inert gas such as Argon is expelled through the path of the arc creating a plasma plume. This both heats and propels the coating material towards the target surface. The design of the gas nozzle and the electrode guide the plume and help maintain an ideal Gaussian profile when the other parameters such as gas flow, carrier gas, gun volts, and amperes are well saturated. However,

several manufacturing disturbances such as nozzle wear, erratic gas flows, consistency in the powder size, and process gas flow leaks can make the plume fluctuate during the coating process.

Several in flight diagnostic tools such as Accuraspray, DPV, and Spray Watch are available to aid the research and development of coating parameters to attain the end properties of the coating faster. However, it should be noted that manufacturing shop floors particularly, SME's cannot afford these tools due to the invasive nature of such diagnostics and the associated skillsets required to make inferences out of these tools. On the other hand, the use of acoustic devices and infrared (IR) cameras has become more widely acceptable due to their easy adoption. Moreover, the data from these can be monitored remotely not only to check the process deviation alarms but also as a closed loop feedback system to digitize the process [7] by integrating them into the process.

Such process deviations could potentially be interfaced with the gas flow controllers, and powder feeder load cells to modify the parameters on the fly depending on the feedback from the acoustic and IR sensors. Deviation of parameters means partial or no melting of particles, reduction of velocity, and plume fluctuation from the Gaussian profile. Such deviation in the particle or plume behaviour will manifest itself in the substrate particle interaction and the generation of acoustic emission will be unique. Considering the speed of particles travelling and the dust ambient conditions, using optical systems to track and monitor particles until splatting has revealed only two parameters such as velocity and temperature being of high importance. In particular, the information about the temperature and heat distribution within the plasma

and the analysis of the plasma shape from this information can lead to an improved understanding of the health of the thermal spray system.

2. Related Work

Several sensing frameworks have been proposed to monitor the plasma and powder to relate their properties to the coating quality. Fauchais et. al. discuss several sensors that can be used to monitor plasma jets including high speed camera systems to monitor plasma symmetry and its fluctuating length showing how its qualities can influence material deposition [8]. Zimmermann et. al. used a high speed camera and a multi-spectral camera setup to investigate the factors that plasma consistency in axial-injection plasma spray [9]. Tiwari et. al. used a similar setup with a high speed CCD camera, an optical fibre, a Photo Multiplier Tube and an oscilloscope to monitor the shape of the plasma in relation to changes in the plasma power [10].

Tracking the coating particles has also been a subject of great interest. Fincke et al. the importance of monitoring the particle temperature distribution which needs to be sufficiently high for particles to more reliably adhere [11]. Multiple studies have shown a correlation between the angle of the spray and changes in mechanical properties such as an increase in porosity, coating thickness and splat morphology ([12],[13], [14], [15]). However, these experiments adjusted the position of the spray head or the coupon to set the spray angle rather than tracking the spray angle in situ. There are several industrial-grade monitoring systems such as Accuraspray, DPV-2000, SprayWatch and Flux Sentinel. These monitor the particle velocities and temperatures via a combination of two-colour pyrometry and CCD cameras processed using specialised algorithms ([16], [17]). The Accuraspray system

can monitor the direction of the powder's travel, but most papers found use it to track particle velocity and temperature distribution.

3. Experimental Setup

Figure 1 is a schematic of the experimental setup used for the experiments. The thermal spray system used an F4MB XL air plasma spray gun made by Oerlikon Metco and a power system that could provide up to 80kW making it capable of melting metals, alloys and ceramics. It was mounted to a 6 axis ABB robot IRB 2400 [18] allowing for complex coating paths. Titanium Metco 4012 A [19] powder was used with a particle size of 40-110 μm. The powder was prepared by an OEM using a sponge titanium melting method making it amenable to be sprayed using the 9MP-CL powder feeder system. The carrier gas used for performing the thermal spray was Argon.

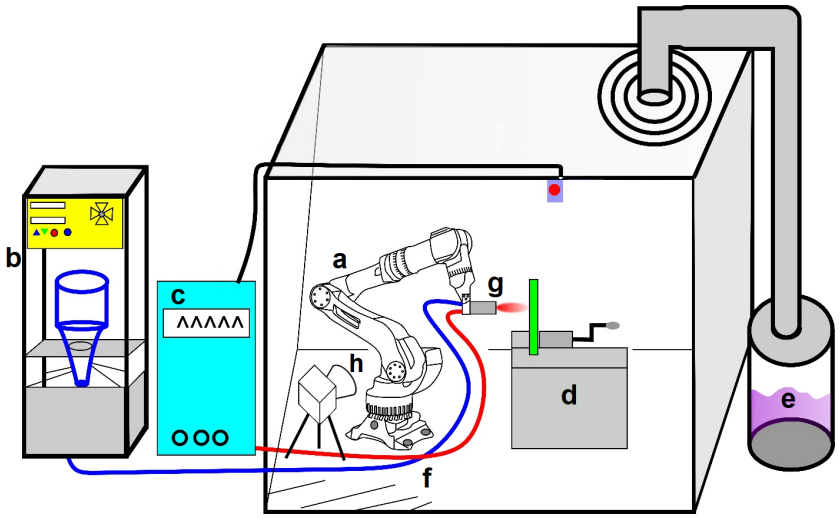

Figure 1: Thermal Spray future on digitalisation adapted from [6]. (a) Robot; (b) Powder feeder; (c) Process control; (d) Specimen holder; (e) Waste powder collector; (f) Feed lines; (g) Plasma torch; (h) FLIR T540 thermal camera

A FLIR camera model T540 [20] was used to monitor the plume in addition to particle temperature. Table 1, Table 2 and Table 3 are a summary of the system specifications, machine settings and experimental plan adopted in this work.

Table 1: Experimental setup specification

Powder name (Vendor Oerlikon)	Titanium Metco 4012 A
Plasma spray gun	F4 Plasma spray gun
Gun Current	550 Amps
Voltage supplied to the gun	18 Volts
Primary gas (Argon)	50 SL/pm Argon @ 140 psi
Spray Distance (mm)	100 mm
Carrier Gas (Argon)	6 SL/pm carrier
Hopper pressure	415 kPa
Blasting	Grit blasted @ 60 psi with 24 grits. Some samples were intentionally used unblasted
Thickness/ pass	10 μm per pass

Table 2: Grit blasting parameters

Blaster Model	Guyson DC 80
Grit Media	Brown Aluminium Oxide
Mesh Size	24
Blast Pressure	0.143 MPa
Blast angle	60 degrees

The experiments were designed to monitor the effects of feed rate and gas flow rate on the powder and plasma plume. The feed rate denotes the target amount of material being fed into the plasma stream. The powder and gas flow rate settings were not measured and were considered to be

Table 3: Parameters used for gas flow experiments

Run	Feed Rate (g/min)	Gas Flow Rate (SL/min)
1	15, 20, 25,30, 35, PULSE	40
2	PULSE, 15, 20, 25, 30, 35	60
3	PULSE, 15, 20, 25, 30, 35	80

correct since the system was freshly calibrated. In Table 3, the use of the word "PULSE" denotes the standard gas flow rate of 10 litres per minute (SL/MIN), compared to the normal 3 SL/MIN. This causes periodic vacuums due to the difference in pressure between each gas "mass" that travels down the pipe.

This affects the feed rate causing it to be more erratic. In manufacturing, this can be caused by several things including a loose O-ring or improperly calibrated equipment. This parameter was tested during the experiments to see if it could be detected.

4. Experimental Results and Analysis

The pre-processing and analysis of the IR imaging data were performed in Python 3.10 [21] and the plots were generated using `matplotlib` [22]. For the thermal spray imaging analysis, the emissivity was set to 0.74 based on the material of the injector holder of the plasma head (Grade 303 Stainless Steel) that is visible in the recordings. This is Item 1 in the F4MB-XL diagram shown in Figure 2 .

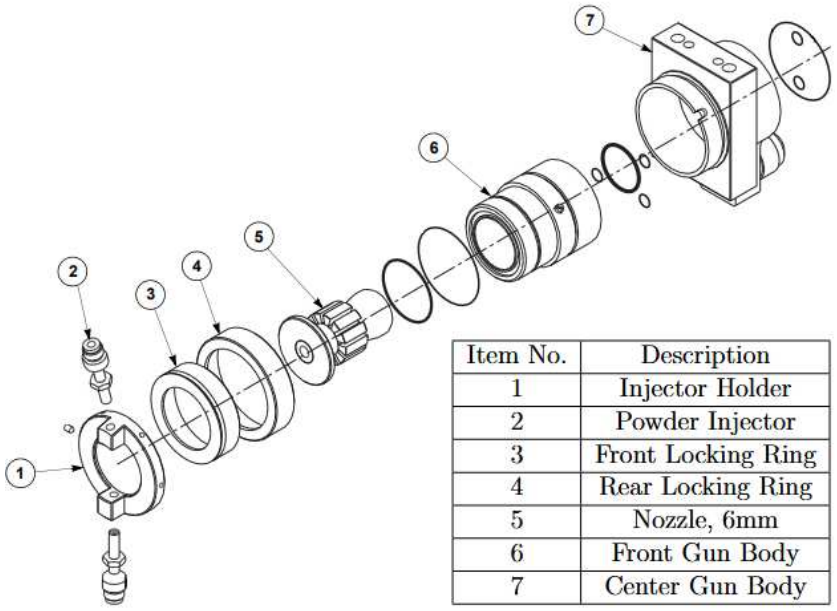

Item No.	Description
1	Injector Holder
2	Powder Injector
3	Front Locking Ring
4	Rear Locking Ring
5	Nozzle, 6mm
6	Front Gun Body
7	Center Gun Body

Figure 2: Assemble of F4MB-XL plasma gun revealing the details of front powder injector. Adapted from [23]

4.1. Initial Observations

The thermal imaging camera recorded the plasma and the in-flight powder particles during spraying (see Fig 3). The nozzle of the plasma gun was placed on the right side of the frame with the plasma gas flow (highlighted in blue) travelling from right to left as indicated in the figure. The two blocks above and below (highlighted in green) are the injector holders of the plasma tool. The powder is injected at the point of the release of plasma which assists in heating and melting the powder and throwing it towards the substrate at a high velocity (highlighted in yellow).

The core of the plasma was hotter than the measurement limit of 1773 °K of the T540 thermal imaging camera used in this research. The pixels associated with those hotter regions were assigned the upper measurement

limit of the colour map.

Under OpenCV's Hot colour map, the core was assigned white colour with hard edges distinguishing it from the edges where the temperature drops off. The background appeared as a singular colour for similar reasons due to the background being at a lower temperature than the lower limit of the sensor. The powder stream was assigned softer edges due to the smaller particles. The temperature for the powder was hottest when coming off the plasma and decreased while travelling far from it. The temperature distribution of the plasma was compliant with the Gaussian distribution. It perceptually loses most of its heat approximately halfway across the frame width. As the travelling speed of each powder exceeds the frame rate of the IR camera and the spatial resolution is not high enough to capture individual particles, the perceived temperature is likely that of the movement of the powder. The powder distribution showed a cone shape due to the top half of the plasma gas pushing upwards and the bottom half pushing downwards causing the powder to diverge. The size of the cone at the end was limited by a combination of the plasma nozzle diameter, the plasma gas flow rate and the material feed rate. The powder's plane of travel, typically known as the coaxial plane, is directed slightly downwards relative to the midline of the plasma core due to the gravity causing an offset or the gas not exerting enough pressure to keep it above the midline.

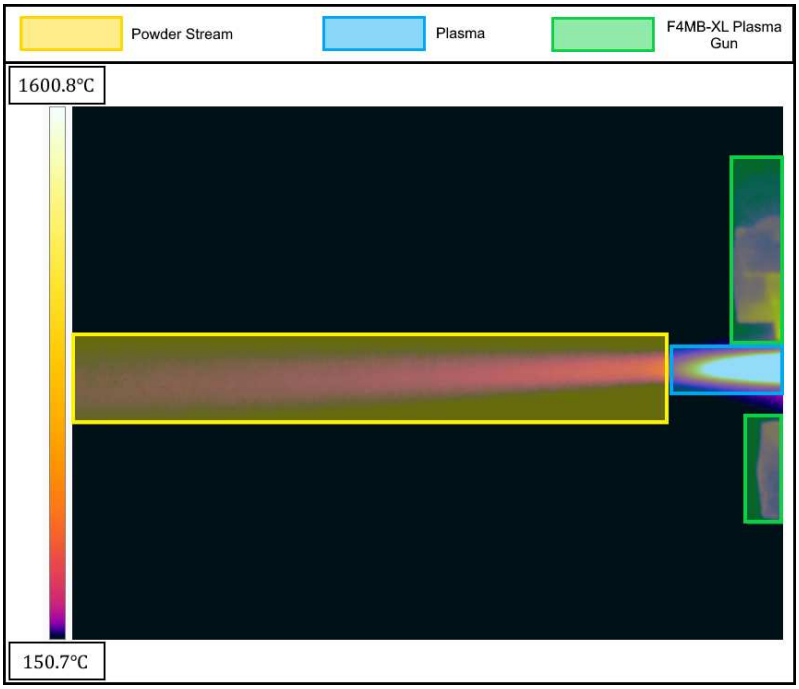

Figure 3: An exemplar thermal image demonstrating typical behaviour captured by the FLIR T540

The thermal camera is also able to detect when the powder deviates from the expected behaviour. Figure 4 shows examples of unusual interactions between the powder and plasma. In Figure 4a, the powder distribution can be seen to spread over a larger area. The tip of the plasma core can be seen to deflect downwards as if the force of the powder is pushing it. For Figure 4b, the powder stream was more skimming on the top of the plasma and the coaxial plane is offset above the plasma.

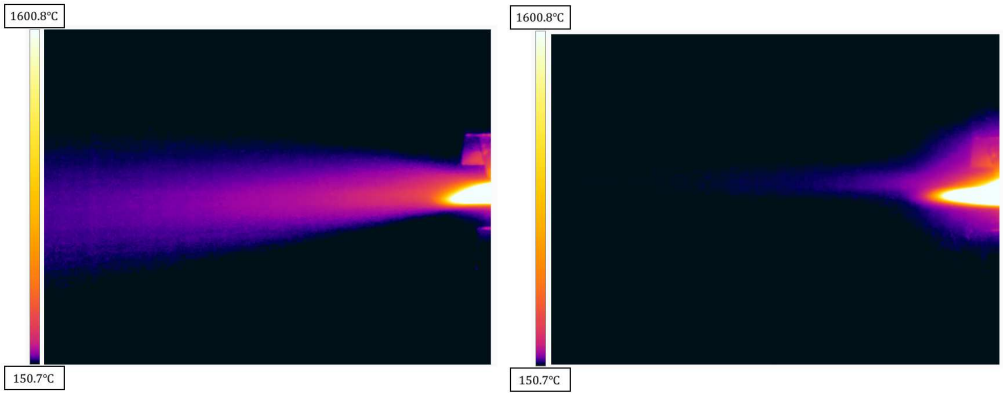

(a) (b)

Figure 4: Examples of suspected powder deflection. In (a) the powder is deflecting off the top of the plasma causing it to be spread over a much wider area than it should be. In (b) the powder is not penetrating the plasma and is instead deflecting off the top meaning it is not being heated

It is suspected that there exists a critical balance between the powder flow rate and the plasma gas flow rate – and its mismatch causes deviations from the nominal behaviour shown in Fig 4. Ideally, the powder should have enough force to be injected into the core of the plasma to get adequately heated up and form a good bond with the surface to be coated. If the repelling force being exerted by the plasma is too strong for the powder, it will deflect off the top meaning the powder is not adequately heated. When the powder flow is too strong, it would travel down through the plasma before the horizontal force of the plasma is enough to eject it. The likely ejection site is in the lower half of the plasma.

4.2. Gaussian Plasma Model

An approach investigated to model the plasma was fitting a Gaussian at the edge of the plasma. Figure 5a illustrates how the plasma can be approximated to be a rotated Gaussian. As the temperature is in an image

coordinate space, the height and standard deviation are in pixels and the coordinates of the mean are along the y-axis. The coordinates of the edge contour can be transformed to be relative to the right side of the image and can be treated as samples of the Gaussian distribution.

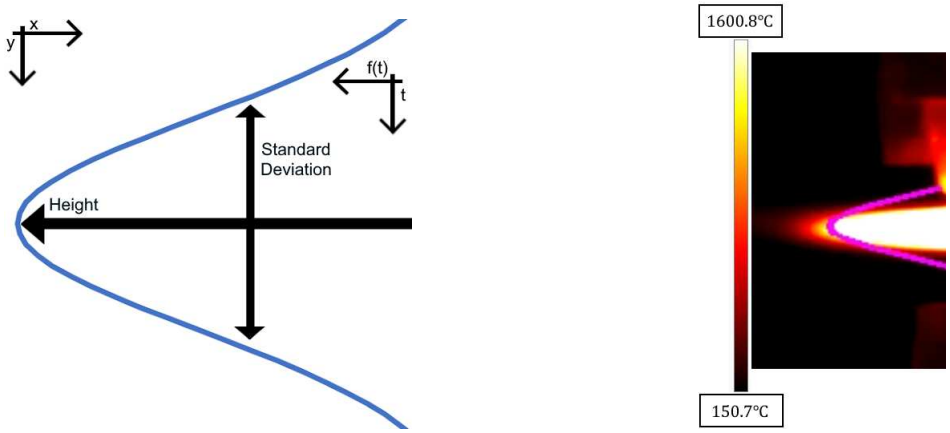

(a) (b)

Figure 5: Theory and example of the developed Plasma Gaussian Model. Figure 5a is a diagram showing the parameters to be identified. Figure 5b is an example of identified Gaussian shown by the magenta line in thermal imaging data of plasma

The height of the Gaussian is taken as the minimum x-coordinate (column) of the contour, identifying the tip of the plasma, minus the width of the frame. The mean of the Gaussian is the y-coordinate (row) where the peak occurs. The standard deviation is calculated from the x-coordinates transformed to be relative to the right side of the image. The parameters identified from processing the thermal images are used in fitting the model described in Equation 1. The coordinate t represents the local coordinates across the base of the Gaussian. The parameter $Scale$ is used to scale the height of the Gaussian so that it matches the height in the image. The μ and $StdDev$ represent the location of the mean and the standard deviation in the

base coordinate space t. The Gaussian base coordinates are then transformed to the image coordinate space by rotating it 90° anti clockwise resulting and then offsetting it with x_0. The y coordinate does not have an offset as μ performs this function.

$$f(t) = \frac{\text{Scale}}{\text{StdDev} * \sqrt{(2\pi)}} exp(-\frac{(t-\mu)^2}{2 * \text{StdDev}^2}) \tag{1}$$

$$x = -f(t) + x_0$$

$$y = t$$

where: t = Coordinate along the base of Gaussian

$Scale$ = Scaling factor to make the height match the data

$StdDev$ = Standard Deviation of the distribution

μ = coordinate of the peak of the distribution in coordinate space t

x, y = Thermal image coordinate space

x_0 = X-coordinate offset

Figure 6 explains the algorithm used to detect and model the plasma. The edge of the plasma can be found by masking the image to the upper 10% values, converting it to grayscale and thresholding the image. This has been found to be effective as the plasma temperature was distinctly higher than the heated material so can be easily identified. Threshold means that the masked area does not cover the outer edges of the plasma where it loses heat to the surrounding environment. Instead, it focuses on the hot "core" of the plasma. The grayscale masked temperature was then converted to

a binary image using OpenCV's implementation of the Otsu threshold [24]. Finally, the contours were identified and the largest one was selected as the plasma.

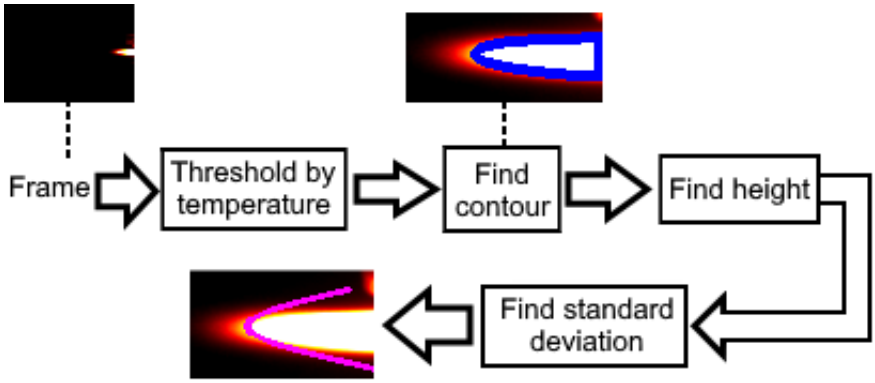

Figure 6: Algorithm for identifying the initial parameter values for modelling the plasma as a symmetrical Gaussian

The model was fitted using `scipy.optimize.curve_fit` [25] with the method set to dogbox and a maximum of 10000 evaluations. The performance of the fitting was evaluated using Root Mean Square Error (RMSE) and Mean Squared Error (MAE) as defined in Equations 2 and 3.

$$MAE(f(x), \hat{f}(x)) = \sum_{i=1}^{N} |f(x)_i - \hat{f}(x)_i| \tag{2}$$

$$\text{RMSE}(f(x), \hat{f}(x)) = \sqrt{\frac{\sum_{i=0}^{N-1}(f(x)_i - \hat{f}(x)_i)^2}{N}} \tag{3}$$

where: $f(x) =$ Identified contour in the image

$\hat{f}(x) =$ Estimated contour from the model

Figure 7 is a plot of the fitting MAE (Figure 7a) and RMSE (Figure 7b) for each of the different gas flow rates. The RMSE and MAE error is zero

when it fails to fit the model or the contour cannot be detected due to the low temperature resulting in an empty masked frame.

The highest MAE and RMSE occur when the plasma is first forming. This is due to the symmetrical model being unable to factor in the asymmetrical transient behaviours previously mentioned. On average the MAE stays between 10-13 for 40 SL/MIN and 60 SL/MIN when the plasma is formed and 8 for 80 SL/MIN. This error is quite small compared to the total area of the image (464 by 348) so the fitting is reasonably accurate overall.

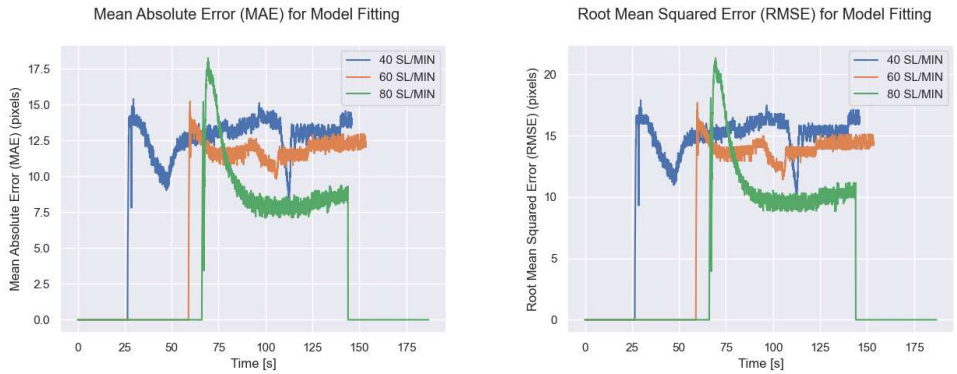

(a) (b)

Figure 7: The RMSE and MAE from fitting Equation 1 to the identified contours in each the thermal image for each of the gas flow rates

Figure 8 shows an example of an identified contour (Figure 8a) and the result from the fitted model (Figure 8b). It is shown to follow the general shape well with no major discrepancies.

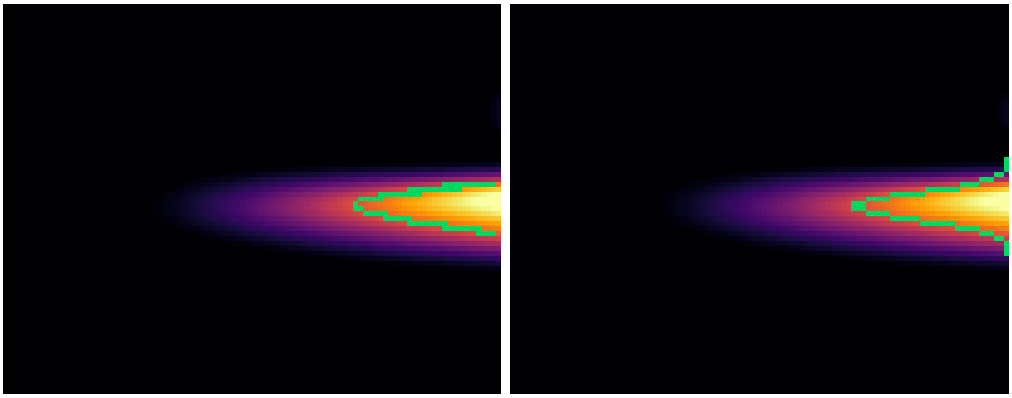

(a) (b)

Figure 8: Example of the identified contour in a frame (a) and the result using the fitted model (b)

One source of error is the contour having multiple height values for the same coordinate, creating perfectly straight lines that are difficult to fit the curved edges of the model. This can be seen in Figure 8a and Figure 8b. Additionally, the contour can have data points that describe the flat base of the Gaussian rather than its body, which would negatively impact the fitting. Also, whilst the plasma forming, the contour has very few data points making achieving an accurate fitting difficult. This is due to the low gas flow rate at the start and the plasma being a certain distance away.

Despite this, the rotated Gaussian model is an efficient representation of the plasma when it has stabilised with good accuracy. A more advanced model would be needed to achieve better accuracy during transient and unstable behaviour modes where it becomes asymmetrical.

4.3. State of the Plasma

As the plasma provides both functions to heat and to force the powder particles, it becomes important to closely monitor the stability of plasma

whilst spraying. One metric is the physical size and temperature distribution of the plasma. If the plasma is too small, the powder may not be heated enough to adhere to the coating surface properly. In the experimental setup, the plasma is generated within a tool head so some masking is required to mask it out so it is not included. In addition, the masking should remove the outer edge of the plasma which is constantly losing to the heat in the environment. They were incredibly fuzzy and would make any estimates of the contour area unstable. The area was to be calculated on the inner, more stable core of the plasma

The ideal temperature threshold was investigated by incrementing it until the tool and the soft edges of the plasma were masked when inspected visually. A value of 1000°C performs well for this experimental setup. The area is calculated by creating a binary mask based on the pixels above the set threshold, finding contours using `cv2.findContours` [26] and selecting the largest which is the plasma.

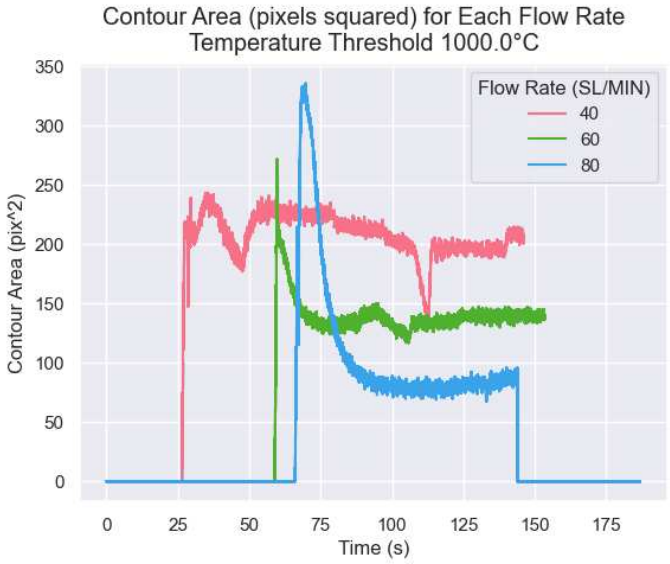

Figure 9: Estimated plasma area over time for different gas flow rates

Figure 9 shows the measured area of the Gaussian distribution over time revealing the influence that the gas flow rate has on the profile of the plasma. Regardless of the gas flow rate, all images show similar transient behaviour. The images show that the plasma initially grew to a larger size before settling into a steady state. The Gaussian Aspect Ratio (GAR) was defined as the Gaussian height divided by the standard deviation. The steady state behaviour once the plasma is formed is then influenced by the different material feed rates when the powder is introduced.

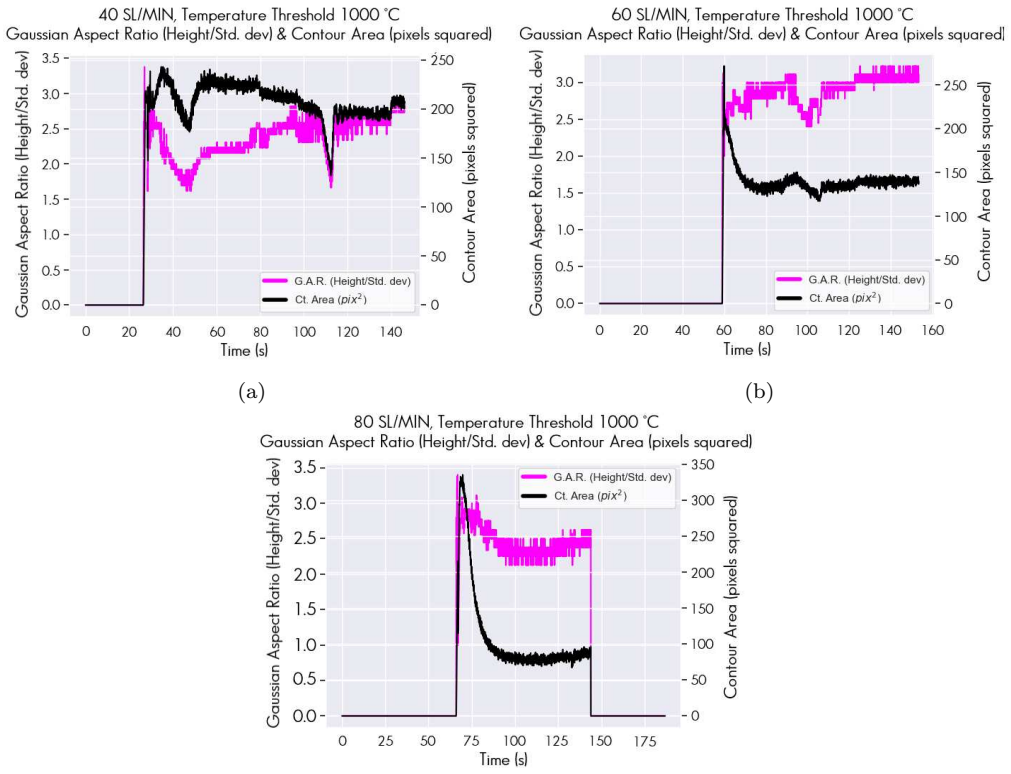

Figure 10: Plot of Gaussian Aspect Ratio (magenta) and plasma Contour Area (black) for the 40 SL/MIN (a), 60 SL/MIN (b) and 80 SL/MIN (c)

Fig 10 shows the evolution of the Gaussian Aspect Ratio (GAR) as a function of different gas flow rates. In theory, as the flow rate increases, the contour area should increase too. As the width of the plasma is confined by the size of the nozzle, the larger area translates to the modelled Gaussian being taller and therefore having a larger GAR. As the gas flow rate increases, the centre of the distribution should move diagonally positively along both axes. The data for 40 SL/MIN remains primarily in a tight region with the distribution centre being primarily between 125 and 250 pixels squared and an aspect ratio between 2 and 2.5. Both the centre and data for 60

SL/MIN, remain in the same contour area range but occupy a higher aspect ratio period between 2.5 and 3.0. During the run using the highest flow rate of 80 SL/MIN, the plasma tool ran out of gas. This is reflected in the Kernel Density Estimate (KDE) (Fig. 11b) showing the plasma mostly having a smaller contour area but a higher aspect ratio of around 3.2 for one distribution peak.

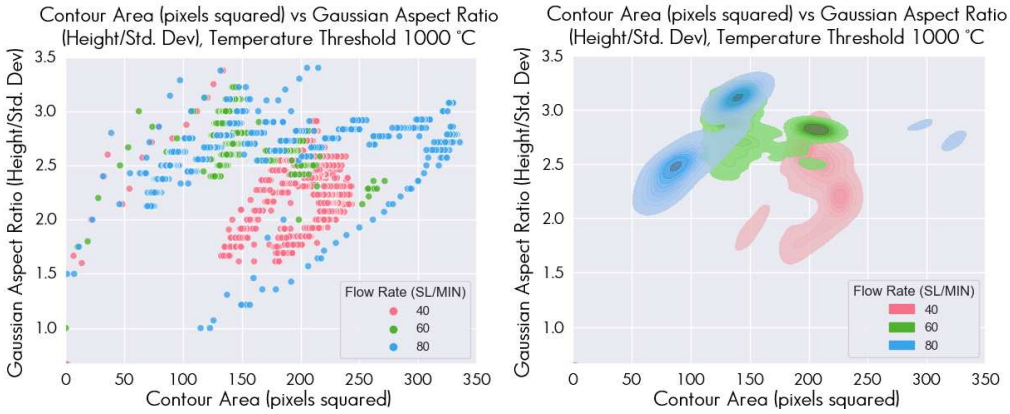

(a) (b)

Figure 11: Scatter (a) and Kernel Density Estimate (b) of Contour Area against Gaussian Aspect Ratio (GAR)

Another feature of great interest is the asymmetry of the plasma. This has been well-studied and shown to affect a wide range of aspects including the temperature distribution which affects how the material is heated, the force distribution which affects the powder deposition ([27], [9],[28]). One feature of a symmetric Gaussian is that the peak is in line with the midpoint of the base. This can be expressed as the angle between the location of the peak and the location of the midpoint. The peak of the Gaussian was the point of the contour furthest away from the right-hand side of the image. The midpoint of the contour was set to row 169 for all recordings. The

angle was found by the `arctan` of the difference in y-coordinate divided by the difference in x-coordinate. The angle was then offset to make 0° the horizontal plane and the absolute value was taken. This metric is called the Asymmetric Angle as non-zero values indicate an asymmetry.

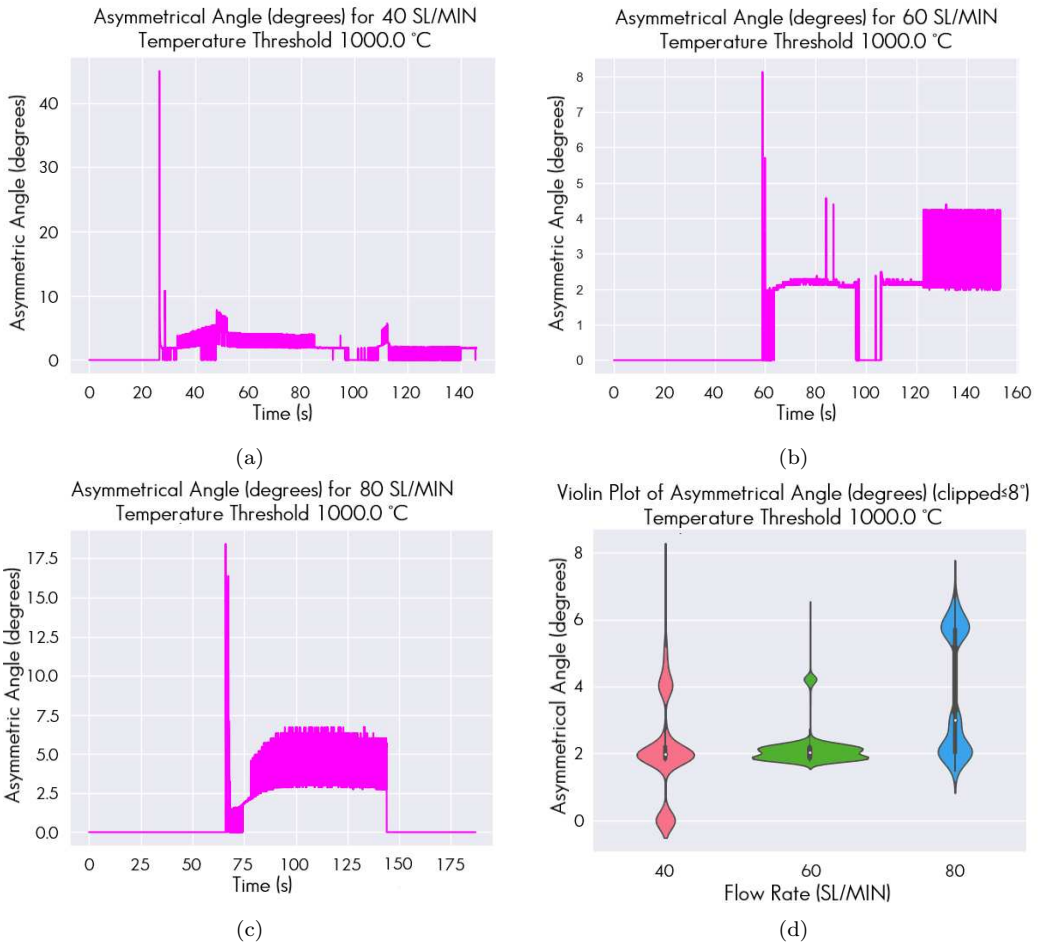

Figure 12: Asymmetric Angle variation for different gas flow rates of 40 SL/min (a), 60 SL/min (b) and 80 SL/min (c) and Violin plot comparison of all asymmetric angles (d)

Figures 12a, 12b and 12c are plots of the asymmetric angle for gas flow rates 40, 60 and 80 SL/min. Figure 12d is a violin plot showing the asymmet-

ric angle distribution for each gas flow rate. The width of the plot denotes the density of values around the corresponding y-axis value. It can be seen that the majority remains mostly at 2.5° for all the feed rates. The flow rate of 60 SL/MIN is the most stable as the majority of the values are around a small, singular value. The instability caused by running out of gas for 80 SL/MIN caused a noticeable proportion of the values to be above 5°.

Capturing the plasma plume with thermal imaging is inherently a difficult challenge. A plasma by its nature has a non-uniform structure meaning properties such as emissivity and density change across its volume. In the case of thermal spray, the shape and density are also affected by the gas flow rate used to create it. Furthermore, during a thermal spray operation, the plasma is being moved around to cover an area introducing motion blur and warping the shape due to momentum.

To get a good quality image and therefore a reliable measurement, the plasma needs to be stationary with its full shape being within the field of view (FOV) of the camera including the origin and the tip. The camera should also be positioned perpendicular to the camera to not introduce any perspective warping. The camera also needs to be positioned as close to the plasma as possible without damaging it to achieve good spatial resolution and therefore accuracy with metrics such as contour area.

The experimental setup satisfies these conditions and also tested the metric under a range of gas flow rates and material feed rates (see Table 3). The angle remained stable within a fixed range whilst the plasma was active. This inherent variance introduced by calculating an angle from an image can also be reduced by applying a smoothing method. Figure 13 shows the estimated

asymmetric angle in blue and the result after applying a rolling mean filter with a window size of 40 samples in orange. The window size was chosen by incrementing the value until the rapid alternating was heavily reduced. A downside of this approach is the slight lag introduced in the smoothed behaviour.

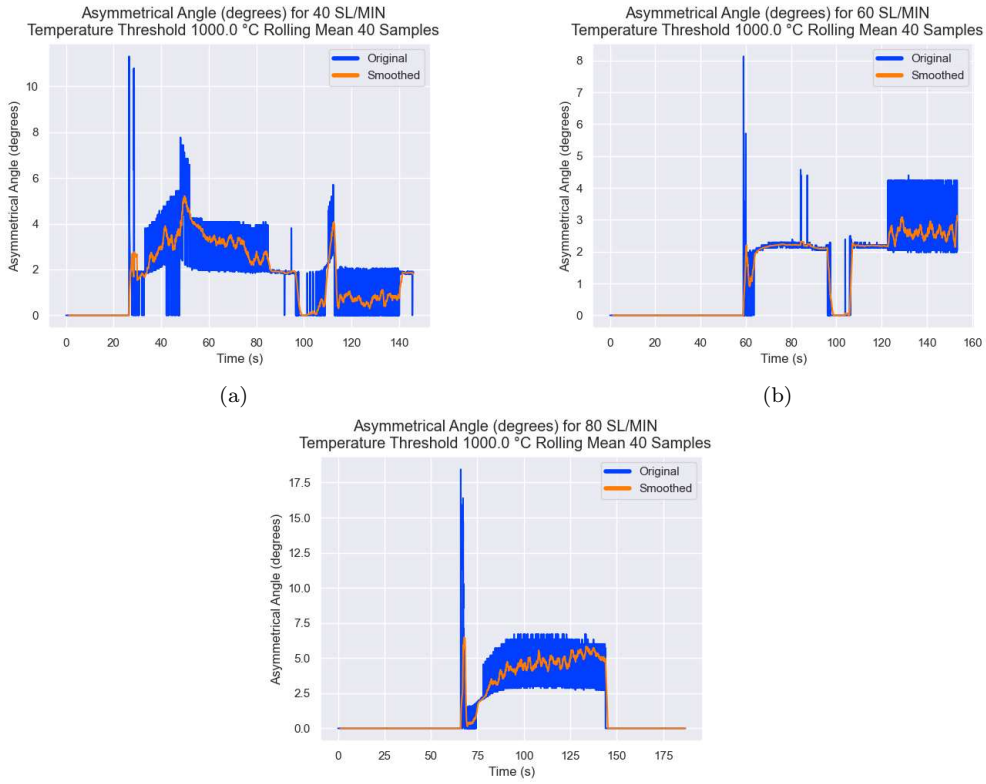

Figure 13: Asymmetric Angle variation for different gas flow rates of 40 SL/min (a), 60 SL/min (b) and 80 SL/min (c) smoothed with a rolling mean filter

4.4. Coaxial Plane

The shape of the powder stream diverges vertically as it is ejected out of the plasma and travels away forming a cone-like shape. The coaxial plane remains largely horizontal and only inclines down at the end of a run. This

is a feature of interest as it relates to how the powder is being utilised and indicates whether the powder reaches the substrate in an intended fashion. If the plane points downwards, then the coating thickness will be thinner and less uniformly distributed as less powder is deposited.

A method was developed to visualise the coaxial plane better using the temperature values. To detect the powder, the emissivity was lowered to 0.1 to raise the sensitivity to changes in the lower temperature range so the powder could be detected. It first breaks the image into non-overlapping windows of size 29 by 29. The size was chosen as it fits equally along the width and height and performed well. In each window, the number of unique values and their frequency was found and the Shannon entropy of these counts was calculated using `scipy.stats.entropy` [29] with the base set to natural log. The idea was to identify the regions of high activity such as the powder stream and the plasma. The background has low entropy typically close to or equal to 0. The location of pixels where the entropy was non-zero were then identified and treated as samples of a line tracing the path of the powder. The normalised entropy of each pixel was also passed as a weight to encourage the line to pass through the high entropy areas. This algorithm is summarised in Figure 14.

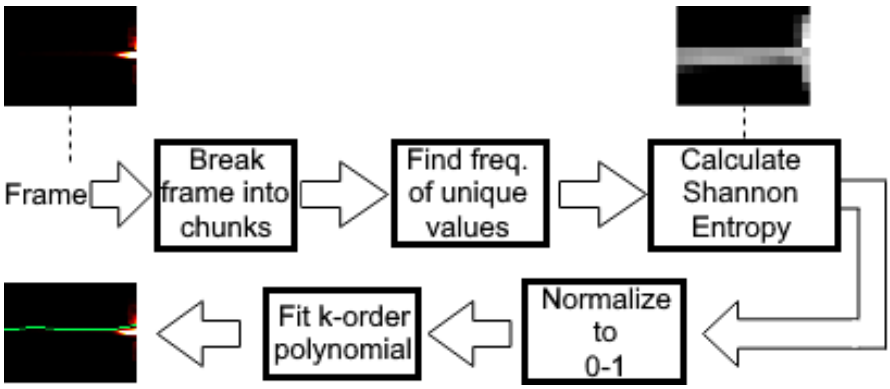

Figure 14: Algorithm for identifying the coaxial plane

Some minor issues of using the approach in Figure 14 can be acknowledged. For instance, with the higher order models, when the plasma is in the field of view and the material stream is not active, the fitted line diverges rapidly towards the top or bottom of the image. Several strategies can be implemented to detect and avoid this. Firstly, as the gradient of the line when the powder is active is going to be close to 0 or slightly negative, a rule can be implemented to ignore gradients that are too large. Secondly, the data could be masked to ignore most of the plasma by ignoring columns above a certain temperature threshold. Finally, a rule can be set to require a certain number of regions to have non-zero entropy. When the powder stream is not active, there are relatively fewer regions with non-zero entropy and they are concentrated around the plasma and tool on one side of the image. A check can be performed by looking at the number of non-zero regions and what proportion of the frame width they cover.

Some additional filters were added to overcome certain issues and make the fitted behaviour adequate. For example, the gap between the top of the plasma and the tool created an area of consistently high entropy. This is due

to the temperature dropping to the background temperature and then rising again to the tool temperature and being recorded as an area of high entropy. This forces the fitted line to pass through it and be at a consistent downward slope.

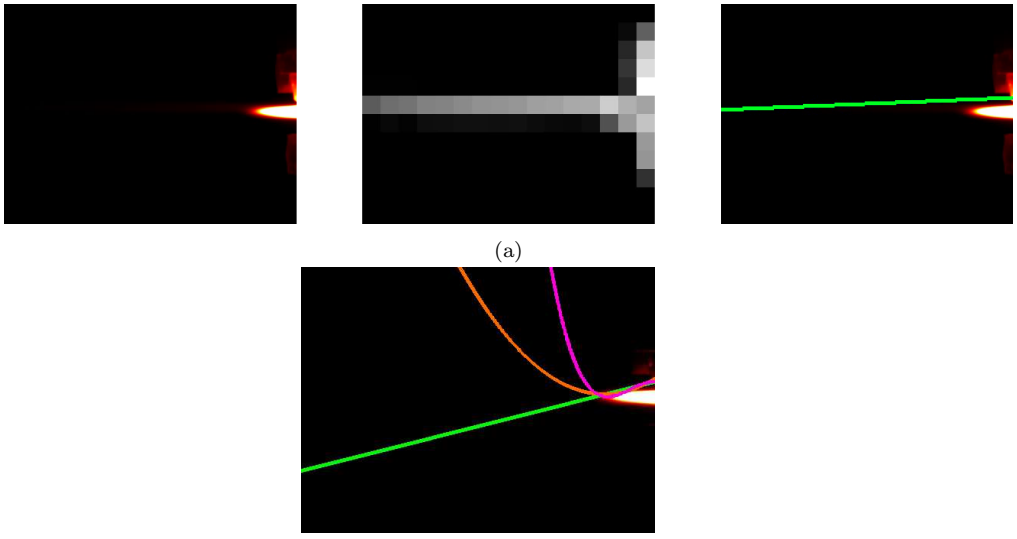

(a)

(b)

Figure 15: Example of the fitted line when the plasma is included. Image (a) shows the different stages of the algorithm. Left is the colour mapped data. The middle image is the entropy converted to grayscale that the line is fitted to. The right image shows the colour mapped data with the fitted line drawn in green

Columns having a maximum temperature larger than 1300°C were set to the minimum temperature of the frame. This eliminates the tool and the majority of the plasma leaving only the edge of the plasma where the powder is being ejected. This is a brute force way of removing it but it is reasonably effective. Masking purely by temperature would include the entire outer edge of the plasma and not fix the issue as it would direct the fitted line to go through the edge. Another undesirable behaviour is when the powder is not active, the fitted line rapidly diverges. It is caused by the line being fitted

to values distributed over a narrow horizontal area. To fit the line through the high entropy areas which are now distributed vertically, it changes its height rapidly. For a 1st order line, this causes the slope to aggressively point towards the bottom of the image. Higher order curves oscillate rapidly with the direction changing between frames. Figure 15b shows an example of this with the 1st, 2nd and 3rd order lines coloured green, orange and magenta respectively.

This can be managed by only fitting curves to when the number of high entropy areas passes a certain threshold. From testing, a minimum number of 8 or more segments performs well. A fixed threshold performs reasonably well, but as the tool surrounding the plasma heats up it introduces more high entropy areas which might get passed the threshold. This can be countered by using the column mask to remove the plasma discussed earlier. Additionally, there is no clear advantage to using higher order polynomials as the main interest is in whether the line dips below the horizontal plane too much causing issues in the spray pattern.

Combining these filters results in a much smoother line when the powder is active as shown in Figure 15b. The angle of the coaxial plane can be calculated by finding the angle between the first and last point of the fitted line. This works best for 1st order fitted lines as the coaxial plane data follows a straight line. For other situations where higher order fittings are better suited, the angle can still be calculated.

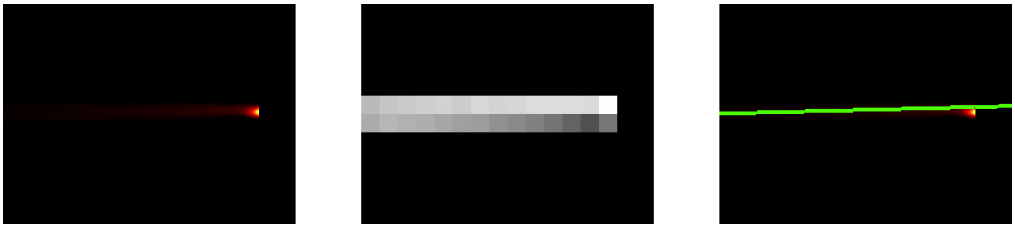

Figure 16: Example of fitted line with discussed filters applied. Left is the colour mapped data after applying the discussed filters. The middle image is the entropy converted to grayscale that the line is fitted to. The right image shows the colour mapped data with the fitted line drawn in green

5. Conclusion

A commercially available thermal camera was integrated into the thermal spray cell to collect information about the plasma temperature distribution and the particle behaviour during a spray process. A series of experiments were performed incrementing the plasma gas flow rate and material flow rate to observe the effect on the process behaviour. The emissivity was set to 0.74 to match the material of the plasma injector head. The plasma was identified by finding the pixels that are above $1000^{c}ircC$ and several metrics were extracted to describe its behaviour.

The most novel metric proposed is called asymmetric angle which is used to monitor the asymmetry of the plasma heat distribution. The angle is calculated as the angle between the physical peak of the distribution and a designated fixed point at its base. Symmetrical heat distribution would have a small angle relative to the horizontal as the temperature distribution above and below will be the same. This novel metric is important as a symmetrical temperature distribution is needed to ensure the majority of particles are heated enough to form a good quality coating.

The plasma was then modelled as a Gaussian whose height and standard

deviation were used to calculate the Gaussian Aspect Ratio (GAR). A relationship was identified between the GAR, the area marked by the contour of the thresholded pixels and the plasma gas flow rate. The shape of the plasma for each gas flow rate occupies a distinct region of the GAR-contour area space. As two of the recordings had documented issues, more data is required to fully separate the effect of the gas flow rate from the equipment issues.

Finally, the angle of travel for the powder stream was estimated. The thermal imaging data was separated into regions and for each, the Shannon entropy was calculated. A polynomial was fitted to the locations of these regions and the entropy to find the path of the material. Additional filters were applied to remove the influence of the plasma to improve the fitting of the line. Different polynomial orders were assessed and a 1D polynomial was found to fit best. The angle between the first and last points of the line gives the angle of travel.

These metrics have opened up some interesting new avenues for investigation. More experiments are needed to collect more data for different gas flow rates to further validate these metrics and improve the understanding of the relationship between them. Another possible approach for future work is applying machine learning to see whether it can more accurately track these metrics and perhaps extract more features of interest.

6. Acknowledgements

This project was funded by the Engineering and Physical Sciences Research Council of the UK through the Intelligent Engineering Coatings for in-manufacture and in-service monitoring of critical safety products (CoatIN)

(EP/T024607/1). The authors would like to acknowledge the Royal Academy of Engineering under the Research Chairs and Senior Research Fellowships scheme and Airbus for their support. Saurav Goel would like to acknowledge the financial support provided by the UKRI via grant EP/S036180/1, the Hubert Curien Partnership Programme from the British Council and the International Exchange Cost Share award by the Royal Society (IEC/NSFC/223536).

7. Data statement

The datasets used and/or analysed during the current study are available and can be downloaded at https://doi.org/10.15131/shef.data.c.7375201

The code is published under the MIT License at https://github.com/D-B-Miller/Trenchcoat

References

[1] D. Tiwari, M. Farnsworth, Z. Zhang, G. W. Jewell, A. Tiwari, In-process monitoring in electrical machine manufacturing: A review of state of the art and future directions, Proceedings of the Institution of Mechanical Engineers, Part B: Journal of Engineering Manufacture 235 (13) (2021) 2035–2051.

[2] D. Tiwari, D. Miller, M. Farnsworth, A. Lambourne, G. W. Jewell, A. Tiwari, Inspection of enamel removal using infrared thermal imaging and machine learning techniques, Sensors 23 (8) (2023) 3977.

[3] J. Verma, G. J. Bennett, S. Goel, Design considerations to fabricate multifunctional superomniphobic surfaces: A review, Vacuum 209 (2023) 111758.

[4] S. Kirthika, G. Goel, A. Matthews, S. Goel, Review of the untapped potentials of antimicrobial materials in the construction sector, Progress in Materials Science 133 (2023) 101065.

[5] V. Venkatachalapathy, N. K. Katiyar, A. Matthews, J. L. Endrino, S. Goel, A guiding framework for process parameter optimisation of thermal spraying, Coatings 13 (4) (2023) 713.

[6] V. Viswanathan, N. K. Katiyar, G. Goel, A. Matthews, S. Goel, Role of thermal spray in combating climate change, Emergent Materials (2021) 1–15.

[7] D. Miller, B. Song, M. Farnsworth, D. Tiwari, F. Freeman, I. Todd, A. Tiwari, Iot and machine learning for in-situ process control using laser based additive manufacturing (lbam) case study, Procedia CIRP 104 (2021) 1813–1818.

[8] P. Fauchais, J. Coudert, M. Vardelle, A. Vardelle, A. Denoirjean, Diagnostics of thermal spraying plasma jets, Journal of Thermal Spray Technology 1 (1992) 117–128.

[9] Z. S., M. G., R. K.H., S. J., Characterization of an axial-injection plasma spray torch, Journal of Thermal Spray Technology 30 (7) (2021) 1724–1736. doi:10.1007/s11666-021-01235-6.
URL https://doi.org/10.1007/s11666-021-01235-6

[10] N. Tiwari, S. Sahasrabudhe, N. Joshi, A. Das, Study of jet fluctuations in dc plasma torch using high speed camera, in: Journal of

Physics: Conference Series, Vol. 208, IOP Publishing, 2010, p. 012134. doi:10.1088/1742-6596/208/1/012134.

[11] J. R. Fincke, W. D. Swank, R. L. Bewley, D. C. Haggard, M. Gevelber, D. Wroblewski, Diagnostics and control in the thermal spray process, Surface and Coatings Technology 146 (2001) 537–543.

[12] S. Leigh, C. Berndt, Evaluation of off-angle thermal spray, Surface and Coatings technology 89 (3) (1997) 213–224.

[13] W. Tillmann, E. Vogli, B. Krebs, Influence of the spray angle on the characteristics of atmospheric plasma sprayed hard material based coatings, Journal of thermal spray technology 17 (2008) 948–955.

[14] G. Montavon, S. Sampath, C. Berndt, H. Herman, C. Coddet, Effects of the spray angle on splat morphology during thermal spraying, Surface and Coatings Technology 91 (1-2) (1997) 107–115.

[15] W. Uczak de Goes, M. Ossiansson, N. Markocsan, M. Gupta, P. Honnerová, Z. Veselỳ, Influence of spray angle on microstructure and lifetime of suspension plasma-sprayed thermal barrier coatings, Journal of Thermal Spray Technology 31 (7) (2022) 2068–2090.

[16] G. Mauer, R. Vaßen, D. Stöver, Comparison and applications of dpv-2000 and accuraspray-g3 diagnostic systems, Journal of Thermal Spray Technology 16 (2007) 414–424. doi:10.1007/s11666-007-9047-2.

[17] G. Mauer, R. Vaßen, D. Stöver, Plasma and particle temperature measurements in thermal spray: approaches and applications, Journal of thermal spray technology 20 (2011) 391–406.

[18] ABB Ltd, IRB 2400 (2024).
URL https://new.abb.com/products/robotics/robots/articulated-robots/irb-2400

[19] Oerlikon Metco, Titanium Metco 4012 A (2024).
URL https://mymetco-europe.oerlikon.com/en-us/product/metco4012a?isRegionSelection

[20] Teledyne FLIR, Flir t540 professional thermal camera (2017).
URL https://www.flir.co.uk/products/t540/

[21] Python Core Team, Python: A dynamic, open source programming language, Python Software Foundation, python version 3.10 (2019).
URL https://www.python.org/

[22] J. D. Hunter, Matplotlib: A 2d graphics environment, Computing in Science & Engineering 9 (3) (2007) 90–95, matplotlib version 3.7.0. doi:10.1109/MCSE.2007.55.

[23] Deha Endustri Kaplama, F4MB-XL Plasma Gun Datasheet (2019).
URL https://dehaendustri.com/wp-content/uploads/PL-97927-EN-13-F4MB-XL-Plasma-Gun-Parts-List-EN.pdf

[24] OpenCV, Opencv: Image thresholding (2023).
URL https://docs.opencv.org/4.x/d7/d4d/tutorial_py_thresholding.html

[25] SciPy, scipy.optimise.curve_fit (2024).
URL https://docs.scipy.org/doc/scipy/reference/generated/scipy.optimize.curve_fit.html

[26] OpenCV, Contours: Getting started (2023).
URL https://docs.opencv.org/4.x/d4/d73/tutorial_py_contours_begin.html

[27] B. P., H. Schubert, J. Uhlenbusch, M. Weiss, Evaporation of zirconia powders in a thermal radio-frequency plasma, Journal of Thermal Spray Technology 10 (4) (2001) 666–672. doi:10.1361/105996301770349196.
URL https://doi.org/10.1361/105996301770349196

[28] S. Mihm, H. Duda, Thomasand Gruner, G. Thomas, B. Dzur, Method and process development of advanced atmospheric plasma spraying for thermal barrier coatings, Journal of Thermal Spray Technology 21 (3) (2012) 400–408. doi:10.1007/s11666-012-9745-2.
URL https://doi.org/10.1007/s11666-012-9745-2

[29] Scipy, scipy.stats.entropy (2023).
URL https://docs.scipy.org/doc/scipy/reference/generated/scipy.stats.entropy.html